

# MAGIA—using atom interferometry to determine the Newtonian gravitational constant

J Stuhler, M Fattori, T Petelski and G M Tino

Dipartimento di Fisica and LENS, Università di Firenze, INFN—Sezione di Firenze,  
Via Sansone 1, I-50019 Sesto Fiorentino (FI), Italy

Received 9 November 2002, in final form 7 February 2003

Published 2 April 2003

Online at [stacks.iop.org/JOptB/5/S75](http://stacks.iop.org/JOptB/5/S75)

## Abstract

We describe our experiment MAGIA (misura accurata di  $G$  mediante interferometria atomica), in which we will use atom interferometry to perform a high precision measurement of the Newtonian gravitational constant  $G$ .

Free-falling laser-cooled atoms in a vertical atomic fountain will be accelerated due to the gravitational potential of nearby source masses (SMs). Detecting this acceleration with techniques of Raman atom interferometry will enable us to assign a value to  $G$ . To suppress systematic effects we will implement a double-differential measurement. This includes launching two atom clouds in a gradiometer configuration and moving the SMs to different vertical positions.

We briefly summarize the general idea of the MAGIA experiment and put it in the context of other high precision  $G$ -measurements. We present the current status of the experiment and report on analyses of the expected measurement accuracy.

**Keywords:** Atom interferometry, Raman interferometry, gravimeter, gradiometer, gravitational constant, precision measurement

## 1. Introduction

Demonstrated for the first time more than 20 years ago, atom interferometers (AIs) [1–4] have developed into very powerful measurement devices with many applications [5]. However, so far only few atom interferometry experiments have been performed to test fundamental physics or to measure fundamental physical constants. Most commonly known, in this context, is the measurement of  $\hbar/m_{\text{Cs}}$  [6], which can be used to determine the fine structure constant  $\alpha$ . Furthermore, atom interferometry has been used to measure the gravitational acceleration on the earth surface  $g$  [7], its vertical gradient  $g'$  [8] and rotations [9].

We will apply the techniques of atom interferometry to determine the Newtonian gravitational constant  $G$ . This fundamental coupling constant was first measured by Cavendish about 200 years ago [10]. Since then, many experiments have aimed at the high precision determination of  $G$ . The motivations for such  $G$ -measurements range

from purely metrological interest through determinations of mass distributions of celestial objects to geophysical applications. In addition, many theoretical models profit from an accurate knowledge of  $G$  [11]. However, despite some 300 measurements [12],  $G$  has remained the least accurately known fundamental physical constant. The 1998 CODATA [13] recommended value of  $G = (6.673 \pm 0.010) \times 10^{-11} \text{ m}^3 \text{ kg}^{-1} \text{ s}^{-2}$  contains an uncertainty of 1500 parts per million (ppm).

Recent measurements with smaller uncertainties of 13.7 ppm [14] and 41 ppm [15] have resulted in  $G$ -values that still disagree on the order of 100 ppm. Hence, there is a strong need for  $G$ -measurements with different methods, which may help to identify possible systematic effects. Note that so far only a few conceptually different methods have resulted in  $G$ -measurements on the level of 1000 ppm or better [12]: the torsion balance, the torsion pendulum, the beam balance and the pendulum cavity. All these methods have in common that masses, which probe the acceleration

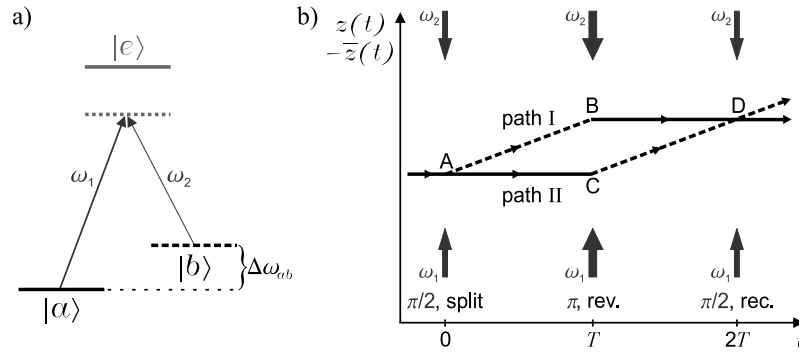


**Figure 1.** Graphical illustration of the Raman atom interferometer. (a)  $\lambda$ -type three-level atom with lower states  $|a\rangle$  and  $|b\rangle$  sharing an excited state  $|e\rangle$ . The Raman lasers have frequencies  $\omega_1$  and  $\omega_2$  slightly below the transition frequencies with a difference that matches the splitting  $\Delta\omega_{ab}$  of the lower states. (b) Scheme of the Raman interferometer: on the vertical axis we plot the atomic vertical position  $z(t)$  after subtracting the free-fall trajectory  $\bar{z}(t)$ . Atom paths are split, reversed (rev.) and recombined (rec.) using a  $\pi/2$ - $\pi$ - $\pi/2$  pulse sequence (see text).

caused by well known source masses (SMs), are suspended, e.g. with fibres. In order to exclude this possible source of systematic effects, one can perform a free-fall experiment. In fact, a determination of  $G$  using a free-falling corner cube has already been performed [16]. However, the uncertainty remained on the order of 1400 ppm.

In order to surpass this result, we are setting up the MAGIA (misura accurata di  $G$  mediante interferometria atomica) experiment [17]. Free-falling  $^{87}\text{Rb}$  atoms forming a vertical Raman atom interferometer [4] will be used to probe the gravitational acceleration originating from nearby SMs. The powerful combination of Raman atom interferometry [18] and laser cooling [19] will allow us to achieve high sensitivity. Using atoms with well known properties, instead of macroscopic probe masses, will help to reduce systematic errors.

The purpose of this paper is the following: we briefly summarize the technique of Raman atom interferometry and show how it can be used to determine  $G$ . Then, we present the set-up of the MAGIA experiment and report on its current status. In addition, we carefully investigate the experimental demands that have to be fulfilled to achieve the 100 ppm targeted accuracy and precision of the  $G$  measurement.

## 2. Raman atom interferometry and its application to determine $G$

Raman atom interferometry (RAI) and its application to detect vertical accelerations of atoms is described e.g. in [7, 18, 20]. Here, we first briefly present the general scheme and the theoretical results. Then we show how one can use RAI to determine  $G$ .

### 2.1. Raman atom interferometry and measurement of vertical accelerations

To measure—as an example for a vertical acceleration—the gravitational acceleration  $g$  on earth using RAI, free-falling atoms within an atomic fountain are illuminated by a sequence of three light pulses. The light pulses are realized with two laser beams, which have frequencies  $\omega_1$  and  $\omega_2$  (see figure 1(a)). The laser beams counter-propagate along the vertical  $z$ -axis with

wavevectors  $\vec{k}_1 = k_1\vec{e}_z$  and  $\vec{k}_2 = -k_2\vec{e}_z$  ( $k_i = \omega_i/c$ ,  $i = 1, 2$ ).  $\omega_1$  and  $\omega_2$  are close to the transitions of a  $\lambda$ -type three-level atom with two lower states  $|a\rangle$  and  $|b\rangle$  and an excited state  $|e\rangle$ . The lasers drive two-photon Raman transitions between  $|a\rangle$  and  $|b\rangle$ . A  $\pi$ -pulse, which has a duration of  $\tau = \pi/\Omega$  ( $\Omega$  being the two-photon Rabi frequency), switches the atomic state from  $|a\rangle$  to  $|b\rangle$  or vice versa. In contrast, a  $\pi/2$ -pulse with duration  $\tau = \pi/(2\Omega)$  splits the atomic wavepacket into an equal superposition of  $|a\rangle$  and  $|b\rangle$ . Besides altering the real amplitudes  $\alpha, \beta$  of the atom's internal wavefunction  $\Psi = \alpha e^{i\Phi_\alpha}|a\rangle + \beta e^{i\Phi_\beta}|b\rangle$ , the light field affects the atoms in two more ways. An atom that changes its internal state receives a momentum transfer by an amount of  $\hbar k_{\text{eff}} = \hbar(k_1 + k_2)$ . At the same time, the phases  $\Phi_{\alpha,\beta}$  are modified according to the local phase of the light field.

Applying first a  $\pi/2$ -pulse, then a  $\pi$ -pulse and finally another  $\pi/2$ -pulse, each separated by the time  $T$ , results in the RAI scheme. This is illustrated in figure 1(b). After recombination of the two paths (path I =  $\overline{ABD}$ , path II =  $\overline{ACD}$ ), the probability  $N_a/N$  of finding the atoms in state  $|a\rangle$  shows a typical interference-like behaviour:

$$N_a/N \propto 1 - \cos(\Phi_I - \Phi_{II}). \quad (1)$$

$\Phi_{I,II}$  are the phases accumulated on paths I and II, respectively. The phases  $\Phi_I$  and  $\Phi_{II}$  depend on the local phase of the light field seen by the atoms during the Raman pulses. This links the vertical atomic position to the phase evolution of the laser field. The phase evolution depends on the effective frequency  $\omega_{\text{eff}}(t) = \omega_1(t) - \omega_2(t)$  and on the phase relation between the Raman pulses. Usually, one varies the effective frequency linearly in time to compensate for the first order Doppler effect of the free-falling atoms. Otherwise, the Raman resonance condition (effective frequency matching the energy splitting of the two lower states) is quickly violated. With  $\omega_{\text{eff}}(t) = \omega_{\text{eff}}(0) - \gamma t$  one obtains

$$\Phi_I - \Phi_{II} = (\gamma - k_{\text{eff}}g)T^2 - \phi(0) + 2\phi(T) - \phi(2T). \quad (2)$$

A proper Doppler effect compensation ( $\gamma = k_{\text{eff}}g$ ) and an unperturbed evolution of the offset laser phase  $\phi$  leads to  $\Phi_I - \Phi_{II} = 0$ . Actively changing the laser phase between  $T$  and  $2T$  by  $\delta\phi$  will result in  $\phi(2T) = \phi(0) + \delta\phi = \phi(T) + \delta\phi$

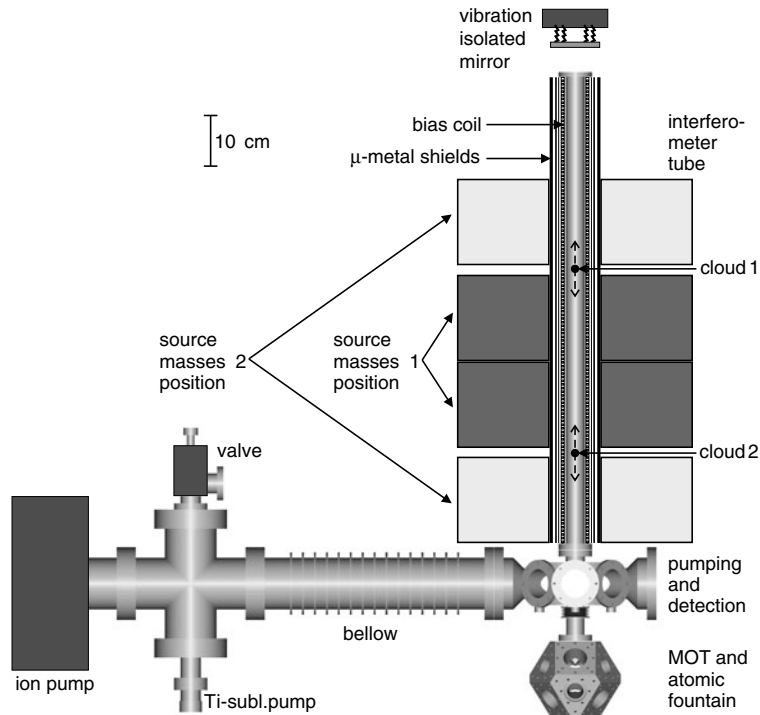


**Figure 2.** Graphical illustration of the experimental set-up with the relevant part of the vacuum system, the atomic trajectories and the source mass positions. Not included are the laser systems, the detection units and the source mass holder. The atomic trajectories during the time of the interferometer pulse sequence are sketched (dashed arrows).

and hence  $\Phi_I - \Phi_{II} = -\delta\phi$ . In this way, one can scan the interference fringe to prove  $(\gamma - k_{\text{eff}}g) = 0$  (for right  $\gamma$ ) or to reveal the phase offset  $(\gamma - k_{\text{eff}}g)T^2$  (for imperfect Doppler compensation). In both cases, the value of  $g$  is obtained combining the measured phase offset and the value of  $\gamma$ , which is set by a frequency generator.

## 2.2. Raman atom interferometry and measurement of $G$

If one adds SMs close to the atomic trajectories, the local acceleration changes due to the gravitational potential of the SMs. Since the amount of change depends on  $G$ , the latter can be determined by an acceleration measurement. However, in order to achieve high sensitivity and accuracy, we will extend this general scheme as will be described in the following.

Firstly, we will launch two clouds of atoms to realize two fountains that are displaced vertically (see figure 2, clouds 1 and 2). The Raman lasers will act on both clouds simultaneously and generate two interferometers at the same time. In a detection of the differential phase shift between the two interferometers, spatial homogeneous accelerations cancel and common mode measurement noise is reduced. The two-cloud set-up results in an atomic gradiometer which allows us to detect the vertical gradient of the gravitational acceleration on earth  $g'$  [8, 22]. If the trajectory of the first cloud is located above the SMs, atoms will experience a SM-induced acceleration in the  $-z$  direction. In contrast, choosing the trajectory of the second cloud below the SMs, the SM-induced acceleration of this cloud will be in the  $+z$  direction. Taking the difference of these two accelerations yields a signal, which is about twice the one obtained with only one cloud.

Secondly, we will determine the differential interferometer phase shifts with the SMs moved to distinct positions (positions 1 and 2, see figure 2). Evaluating the difference between those measurements will further reduce systematic errors if their origins are constant during the timescale of the SM repositioning. One example for such a removable systematic error is the effect arising from spatially inhomogeneous accelerations like the earth's gravity gradient  $g'$ .

Thirdly, choosing well adapted atomic trajectories and source mass positions will reduce dramatically the experimental demands, like precision and stability of the atomic fountains, that have to be fulfilled to achieve the targeted accuracy of  $\Delta G/G \approx 10^{-4}$ . Note that e.g. due to  $g'$  a vertically displaced atomic fountain detects a modified vertical acceleration. This mimics an acceleration caused by the SMs and leads to a systematic error. With a SM-induced acceleration of less than  $10^{-6} \text{ m s}^{-2}$  and  $g' = 3 \times 10^{-6} \text{ s}^{-2}$ , a measurement accuracy of 100 ppm requires a launch accuracy better than  $30 \mu\text{m}$ . In contrast, if the atomic trajectories lie in regions where  $g'$  is (nearly) compensated by the SM gravitational potential (see section 4), even vertical displacements on the order of 1 mm can be tolerated.

The combination of these three modifications will allow us to reach an accuracy of better than 100 ppm when using RAI to determine the Newtonian gravitational constant.

## 3. The MAGIA set-up and its current status

The MAGIA experiment will be performed using  $^{87}\text{Rb}$  atoms because they are well suited for laser cooling and atom interferometry. Compared to caesium, rubidium has the

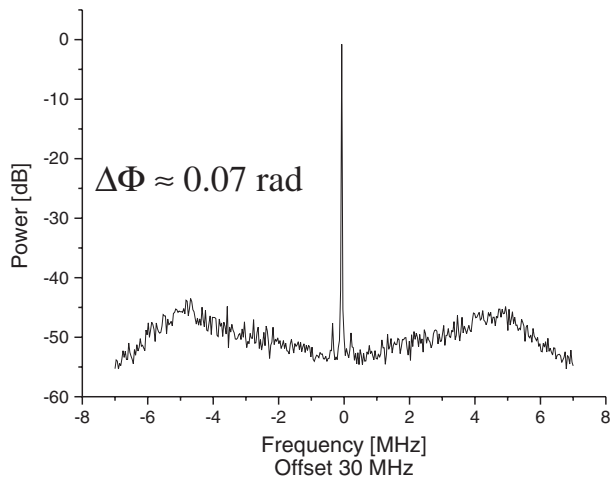


**Figure 3.** Beat note of the phase-locked diode lasers that are used for the Raman pulses. The signal is taken after the first mixing stage and detected with a spectrum analyser. The resolution bandwidth is 3 kHz and no averaging has been performed.

advantage of a smaller collisional shift of the transition frequencies (a well known problem in Cs atomic fountain clocks). Furthermore, rubidium has two stable isotopes and can be Bose–Einstein condensed easily leaving the way open for further extensions of the experiment. In this section we will describe the laser systems, the vacuum system and the source mass design.

### 3.1. Laser systems

All the lasers used in the experiment are close to transitions from the two lowest hyperfine states  $5^2S_{1/2}$ ,  $F = 2$  and  $5^2S_{1/2}$ ,  $F = 3$  of  $^{87}\text{Rb}$  to the  $5^2P_{3/2}$ ,  $F = 0, 1, 2, 3$  manifold. The corresponding wavelengths are around 780 nm. To trap, launch and detect Rb atoms, we use grating stabilized diode lasers. They are locked to atomic transitions using standard spectroscopy techniques or a Doppler-free dichroic atomic vapour laser lock [23]. If necessary, the lasers are amplified in master–slave configurations with the slave being either a high power laser diode or a tapered amplifier. Frequency modification and amplitude control of the laser light is achieved using acousto-optical modulators.

The lasers for the Raman pulses are a critical part of the atom interferometer experiment. Note that the light field—more precisely the relative phase between the two lasers that drive the two-photon Raman transitions between  $|a\rangle = |5^2S_{1/2}, F = 2, m_F = 0\rangle$  and  $|b\rangle = |5^2S_{1/2}, F = 3, m_F = 0\rangle$ —is used as a ruler to measure the free-fall of the atoms. Random variations of this relative phase will therefore show up as noise in the acceleration measurement and could limit the precision in determining  $G$ . For the Raman pulses we have also set up grating stabilized laser diodes. However, to avoid uncontrolled variations of their relative phase and to stabilize a difference in frequency of about 6.8 GHz between them, we have implemented an optical phase-lock loop (OPLL) [24]: the two lasers are overlapped and partly sent on to a fast photodiode. The detected beat signal is then mixed down to low frequencies in two stages. The resulting signal is proportional to the phase difference between the two lasers and can be used

to stabilize their relative phase. Figure 3 shows the detected beat signal of the phase-locked lasers after the first mixing stage. Already our first version of the OPLL proved to be very stable. As can be estimated from the presented beat note signal, the OPLL results in an error of the phase between the two lasers on the order of  $\Delta\Phi \approx 0.07$  rad. Currently, we are setting up an improved OPLL and an amplification stage of the Raman lasers using a tapered amplifier.

### 3.2. Vacuum system

The relevant part of the vacuum system is shown in figure 2 together with the SM positions and the atomic trajectories. It mainly consists of three parts. In the lowest part—a titanium cube with cut edges—atoms will be trapped, cooled and launched vertically using a magneto-optical trap and moving optical molasses. The six independent laser beams are chosen to be in a 1–1–1 six-beam  $\sigma^+/\sigma^-$  configuration. This keeps the central vertical axis free for the Raman laser beams and allows us to realize a stable and precise atomic fountain [25].

The second part of the vacuum system is a 316 LN stainless steel cell with several welded tubes. This cell is used for pumping and to detect the atoms. Furthermore, it guarantees additional optical access to implement degenerate Raman cooling in a co-moving frame [26] while the atoms traverse the cell during their way up to the top of the vacuum system. Degenerate Raman cooling can be used as a second cooling and acceleration stage to increase the brightness of the atomic fountain.

The interferometer tube on top of the vacuum system is 1 m long, has a diameter of 40 mm and is made of titanium. The Raman laser beams enter the vacuum system from below at the central axis of the lower cube and leave the interferometer tube at the top through a high quality window. They pass a quarter-wave retardation plate, are reflected from a vibration isolated mirror and re-travel all the way back down. The actual Raman laser pulses are applied while the atoms are on their free-fall parabola within the magnetically shielded interferometer tube.

### 3.3. Source masses

The SMs will be two separate major discs of a high density material. Choosing the tungsten alloy Densimet 180 K, each major disc will have an inner diameter of  $\sim 0.10$  m, an outer diameter of  $\sim 0.44$  m and height of  $\sim 0.18$  m. With a density of  $18\,000\text{ kg m}^{-3}$  this results in a mass of about 500 kg per major disc. Besides the high density, this tungsten alloy has the advantages of a high uniformity<sup>1</sup>, a low thermal expansion coefficient of  $5.3 \times 10^{-6}\text{ K}^{-1}$  and a high resistivity of  $0.18\ \mu\Omega\text{ m}$ . The latter ensures fast eddy current damping. Furthermore, this alloy is hard and can be machined quite easily and precisely.

The SMs in position 1 (see figure 2, dark grey boxes) generate a vertical acceleration  $a(z)$  on the central axis as plotted in figure 4(a). The maximum acceleration is  $a_{\text{max}} \approx 9 \times 10^{-7}\text{ m s}^{-2}$ . Taking the earth gravity gradient  $g' \approx 3 \times 10^{-6}\text{ s}^{-2}$  into account,  $a(z)$  changes significantly (figure 4(b)). In this plot, we also indicate the projected atomic trajectories

<sup>1</sup> Of the order of 5 parts in 10000 [27].

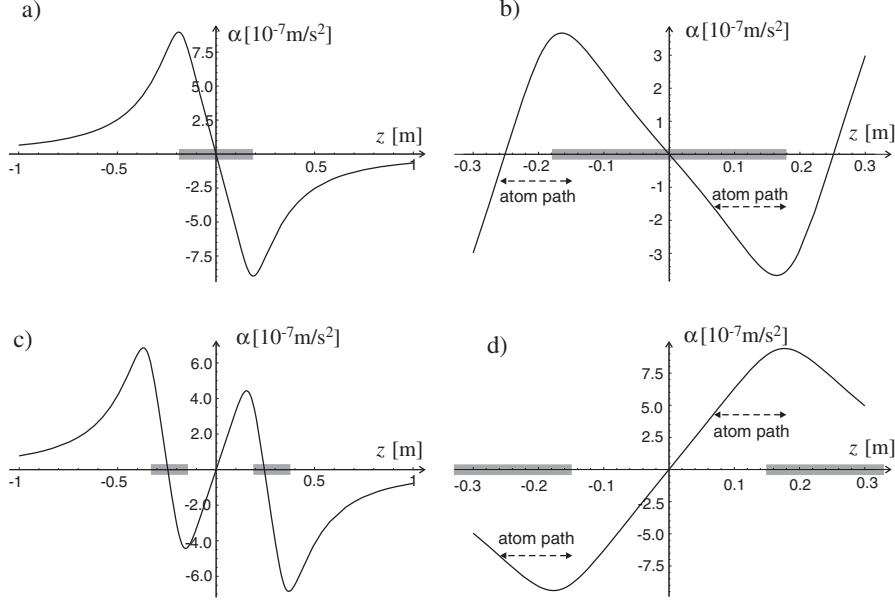


**Figure 4.** Calculated on-axis vertical acceleration  $a(z)$  with the two 500 kg SMs in positions 1 (a), (b) and 2 (c), (d) (see figure 2). The grey boxes illustrate the vertical position of the SMs. (a), (c)  $a(z)$  without the effect of  $g$  and  $g'$ . (b), (d)  $a(z)$  with the effect of  $g'$ . The dashed arrows mark the projected atomic trajectories.

that include an extremum of the acceleration due to the SMs and  $g'$ . The choice of these trajectories guarantees a reduced sensitivity of the resulting atomic phase shift on variations of initial conditions, like atomic position and velocity. This is essential for the achievement of high accuracy and high precision in the  $G$ -measurement (see section 4). Moving the SMs to position 2 (figure 2, light grey boxes) changes the sign and the magnitude of the SM-induced acceleration (see figures 4(c) and (d)) in such a way that, together with the unchanged atomic trajectories, the atomic phase shift remains only weakly dependent on variations of initial conditions.

#### 4. Expected accuracy

In this section, we present numerical studies on possible resolution and accuracy limits of our measurement. We concentrate on the combination of a spatially inhomogeneous acceleration—caused by the SMs,  $g'$  and  $g$ —and atom clouds with a spread in the initial positions and velocities of the atoms. Furthermore, we study systematic effects arising from errors in the mean initial velocity and/or position of the clouds as well as the influence of imperfect SM positioning. The analyses are performed for a pulse separation time of  $T = 150$  ms, which corresponds to a vertical free-fall distance of about 0.11 m. They lead to optimal atomic trajectories and SM positions that reduce the effects of a non-zero cloud size, a spread in atomic velocity and deviations of the cloud's central position or its mean velocity from the optimal values. We then give constraints of experimental parameters that allow us to achieve the targeted accuracy of  $\Delta G/G \approx 10^{-4}$ . Other sources of noise in a Raman atom interferometer have already been studied comprehensively [21, 22] and will be greatly suppressed due to the double-differential method of measurement.

Our investigations are based on the phase shift detected by one  $^{87}\text{Rb}$  atom (or one single Raman interferometer). To

determine this phase shift  $\Phi_i = \Phi_{\text{I},i} - \Phi_{\text{II},i}$  (section 2.1,  $i = 1, 2$  is as in figure 2 numbering the cloud the atom belongs to), we calculate numerically the atomic free-fall parabola taking into account  $g$ ,  $g'$  and the acceleration caused by the SMs. Knowing the space–time points of the atom, we determine the phases imprinted onto the atomic wavefunction at each of the infinitely short Raman pulses and evaluate  $\Phi_i$ .

##### 4.1. Optimal atomic trajectories, source mass positions and detection signal

Generally,  $\Phi_i$  depends strongly on the SM positions as well as on  $\vec{x}_{0,i}$  and  $\vec{v}_{0,i}$ , the atomic position and velocity at  $t = 0$  when the first Raman pulse is applied. However, calculating  $\Phi_i$  for different  $\vec{x}_{0,i}$  and  $\vec{v}_{0,i}$  but with the SMs fixed to position 1 (figures 2 and 4), we find *optimal atomic trajectories* (characterized by  $\vec{x}_{0,i}^{\text{opt}}$  and  $\vec{v}_{0,i}^{\text{opt}}$ ). They include a local extremum of the acceleration and result in a phase shift that is relatively insensitive to variations of the initial atomic position and/or velocity.

With the obtained  $\vec{x}_{0,i}^{\text{opt}}$  and  $\vec{v}_{0,i}^{\text{opt}}$  we then investigate different SM positions. In this way, we find the *optimal position 2* of the SMs. It is the one that leaves  $\Phi_i$  the most insensitive against small variations in the (unchanged!) initial atomic conditions. Optimizing the exact position 2 of the SMs instead of finding new optimal atomic trajectories eases the experimental procedure. Since one can use the same  $\vec{x}_{0,i}^{\text{opt}}$  and  $\vec{v}_{0,i}^{\text{opt}}$  for both SM positions, the launch of the atoms does not have to be modified.

Taking *ideal clouds* with atoms that all have optimal initial atomic conditions, we calculate the *optimal phase shifts*  $\Phi_i^{\text{opt}}$  and determine  $\Delta\Phi^{\text{pos1}}$  and  $\Delta\Phi^{\text{pos2}}$ , the differences in the optimal phase shifts of the two interferometers for the SMs in positions 1 and 2, respectively. Subtraction of these results gives the overall differential signal  $S = \Delta\Phi^{\text{pos2}} - \Delta\Phi^{\text{pos1}} \approx$

**Table 1.** Acceptable ranges of experimental parameters that still allow us to achieve the targeted accuracy of  $\Delta G/G < 10^{-4}$  (100 ppm).  $\Delta z_0(\Delta v_{z_0})$  ( $\Delta r_0(\Delta v_{r_0})$ ) is the tolerable offset of the initial mean vertical (radial) position depending on the offset in the vertical (radial) velocity. ‘SM pos. accuracy’ is the demanded accuracy in the positioning of the SMs (also after moving). ‘SM pos. knowledge’ is the knowledge of the distance between the SMs. The calculations were performed for atomic clouds with  $\sigma_{z,r} = 1$  mm and  $\sigma_{v_{z,r}} = 1 v_{\text{rec}}$ . Noise due to the light field and the detection has been omitted.

$\Delta z_0$ ( $\Delta v_{z_0} = 0$ )	$\Delta r_0$ ( $\Delta v_{r_0} = 0$ )	$\Delta z_0$ ( $\Delta v_{z_0} = 0.5 v_{\text{rec}}$ )	$\Delta r_0$ ( $\Delta v_{r_0} = 0.5 v_{\text{rec}}$ )
$\pm 1.2$ mm	$\pm 1.7$ mm	$\pm 0.8$ mm	$\pm 1.2$ mm
$\Delta z_0$ ( $\Delta v_{z_0} = v_{\text{rec}}$ )	$\Delta r_0$ ( $\Delta v_{r_0} = v_{\text{rec}}$ )	SM pos. accuracy	SM pos. knowledge
$\pm 0.4$ mm	$\pm 0.7$ mm	$\pm 0.1$ mm	$\pm 0.01$ mm

0.9 rad. Note that contributions of  $g$  and  $g'$  cancel and that  $S$  depends linearly on  $G$ .

#### 4.2. Effects of non-zero cloud size and velocity distribution of the atoms

*Real clouds* contain atoms with different vertical and radial positions ( $z, r$ ) and with different vertical and radial velocities ( $v_z, v_r$ ). The measured phase shift of one cloud is the weighted average over all the individual atomic phase shifts. We model real clouds considering Gaussian atomic density and velocity distributions, centred around the optimal initial values  $\bar{x}_{0,i}^{\text{opt}}$  and  $\bar{v}_{0,i}^{\text{opt}}$ . The corresponding  $1/\sqrt{e}$  full widths of the distributions are  $2\sigma_z, 2\sigma_r, 2\sigma_{v_z}$  and  $2\sigma_{v_r}$ . The individual atomic phase shifts are calculated as described above but taking into account their different initial conditions. Then we perform the weighted average to obtain the one-interferometer phase shift  $\langle \Phi_i \rangle$  and compare it to  $\Phi_i^{\text{opt}}$ , the value for atoms with optimal initial conditions. For non-zero widths of the Gaussian distributions  $\langle \Phi_i \rangle$  differs from  $\Phi_i^{\text{opt}}$ .

We find that for  $\sigma_{v_z} < 1 v_{\text{rec}} \approx 6$  mm s<sup>-1</sup>, the difference between  $\langle \Phi_i \rangle$  and  $\Phi_i^{\text{opt}}$  is less than 100 ppm if  $\sigma_z < 1$  mm. Smaller values of  $\sigma_{v_z}$ , which correspond to a lower temperature of the cloud or a more severe velocity selection, allow even bigger cloud sizes. It is worthwhile to mention that the amount of deviation is predictable. Knowing experimentally e.g. the cloud size to within 10% allows us to achieve an accuracy of 100 ppm even for vertical cloud sizes of  $\sigma_z \approx 2.2$  mm. Similar results are found for the radial velocity and density distributions. There, the cloud size can be as large as  $\sigma_r \approx 1$  mm for  $\sigma_{v_r} < 1 v_{\text{rec}}$ . Again, lower values of  $\sigma_{v_r}$  allow even larger cloud sizes and  $\langle \Phi_i \rangle - \Phi_i^{\text{opt}}$  can be calculated.

As a second effect besides the deviation of the averaged phase shift from the ideal one, atoms with different initial conditions show dephasing. This leads to a reduction of the fringe visibility. Our calculations show that for cloud sizes and velocity spreads well above the given values, the corresponding reduction in the  $S/N$ -ratio is negligible. Note that limited by other noise sources, like quantum projection noise [28], we aim at a 1%  $G$  resolution per single measurement. Averaging 10 000 measurements should then allow us to reach 100 ppm.

#### 4.3. Systematic errors due to cloud central position and mean velocity

Systematic errors can also arise from offsets ( $\Delta z_0, \Delta r_0, \Delta v_{z_0}$  and  $\Delta v_{r_0}$ ) in the central initial vertical or radial position or in the mean vertical or radial velocity of the atomic cloud. Such offsets may arise from an imperfect launch of the atoms and will lead to  $\langle \Phi_i \rangle - \Phi_i^{\text{opt}} \neq 0$ . This results in a systematic

misinterpretation of the value for  $G$ . To analyse these effects, we consider clouds with  $\sigma_r = \sigma_z = 1$  mm and  $\sigma_{v_r} = \sigma_{v_z} = 1 v_{\text{rec}}$  and vary their central position and mean velocity. From the calculations we find acceptable ranges for  $\Delta z_0, \Delta r_0, \Delta v_{z_0}$  and  $\Delta v_{r_0}$  that allow us to reach the targeted accuracy of 100 ppm. Table 1 shows the tolerable offsets in the cloud position for several offsets in the mean velocity of the cloud. We also include the demands on the SM positioning.

From table 1 one can see the following. A cloud (with size  $2\sigma = 2$  mm and velocity spread  $2\sigma_v = 2 v_{\text{rec}}$ ) can have an offset in the initial vertical (radial) central position as large as 0.4 mm (0.7 mm) even if at the same time the corresponding velocity deviates by  $1 v_{\text{rec}}$  from the optimal value. Still it allows us to reach an accuracy of 100 ppm. Smaller systematic errors in the initial velocity reduce the demands on the initial position even further. The dramatic reduction of the experimental constraints is achieved by the proper choice of SM positions and atomic trajectories. Note that otherwise (section 2.2) e.g. the vertical central position of the cloud would have to be exact to within approximately 30  $\mu\text{m}$ . However, the reduced sensitivity to atomic initial conditions comes at the price of a precise knowledge (0.01 mm) of the vertical distance between the SM positions and an accurate vertical movement of the SM (to 0.1 mm). Although quite demanding, controlling and measuring the relative SM positions to this accuracy can be done.

Many other sources of noise and systematic errors will cancel due to the double-differential method of measurement (two interferometers and two SM positions). Only error sources that affect both clouds differently *and* that are not constant in time would lead to a misinterpretation of the  $G$ -value. The relevant timescale for the constancy of such error sources is *not* given by the overall measurement time of several hours *but* by the time which is needed to perform a full double-differential measurement. This time is mainly determined by the SM repositioning and will be on the order of a minute.

## 5. Conclusion

We have described the general idea of the MAGIA experiment, in which we will apply techniques of atom interferometry to determine the Newtonian gravitational constant  $G$ . The free-fall of <sup>87</sup>Rb atoms within an atomic fountain will be perturbed by the gravitational potential of nearby source masses. This perturbation depends on the mass distributions and on the value of  $G$ . We will detect the change in the vertical acceleration using two Raman atom interferometers in a gradiometer configuration. To suppress systematic errors, we will perform measurements with different source mass positions. We have presented the experimental set-up,

which is already partly functioning. We have numerically analysed the influence of atomic initial conditions and source mass locations on the measurement, and found ideal atomic trajectories. The obtained results are encouraging to determine  $G$  with an accuracy on the order of 100 ppm. Further improvements may involve atomic Bose–Einstein condensates or the implementation of optical dipole traps. Using modified configurations, atom interferometry can be applied to prove the  $1/r^2$ -dependence of Newton’s law of gravitation at short distances or to test the equivalence principle.

## Acknowledgments

We thank Mark Kasevich for stimulating discussions and appreciate fruitful suggestions of Achim Peters and James Faller. JS and TP acknowledge support from the European Union under contract number HPRI/CT/1999/00111. This work is financed by the Istituto Nazionale di Fisica Nucleare (INFN).

## References

- [1] Carnal O and Mlynek J 1991 *Phys. Rev. Lett.* **66** 2689–92
- [2] Keith D W, Ekstrom C R, Turchette Q A and Pritchard D E 1991 *Phys. Rev. Lett.* **66** 2693–6
- [3] Riehle F, Kisters Th, Witte A, Helmcke J and Bordé Ch J 1991 *Phys. Rev. Lett.* **67** 177–80
- [4] Kasevich M and Chu S 1991 *Phys. Rev. Lett.* **67** 181–4
- [5] For an overview on atom interferometry see Berman P R (ed) 1997 *Atom Interferometry* (New York: Academic) and references therein Pritchard D E, Cronin A D, Gupta S and Kokorowski D A 2001 *Ann. Phys., Lpz.* **10** 35–54
- [6] Weiss D S, Young B C and Chu S 1993 *Phys. Rev. Lett.* **70** 2706–9
- [7] Peters A, Chung K Y and Chu S 1999 *Nature* **400** 849–52
- [8] Snadden M J, McGuiirk J N, Bouyer P, Haritos K G and Kasevich M A 1998 *Phys. Rev. Lett.* **81** 971–4
- [9] Gustavson T L, Landragin A and Kasevich M A 2000 *Class. Quantum Gravity* **17** 2385–97
- [10] Cavendish H 1798 *Phil. Trans. R. Soc.* **88** 467
- [11] A comprehensive listing of motivations for  $G$  measurements can be found in Gillies G T 1997 *Rep. Prog. Phys.* **60** 151–225
- [12] For a recent review of the status of  $G$  measurements see e.g. Luo J and Hu Z-K 2000 *Class. Quantum Gravity* **17** 2351–63
- [13] Mohr P J and Taylor B N 2000 *Rev. Mod. Phys.* **72** 351–495 The CODATA values can also be found at <http://physics.nist.gov/cuu/Constants/index.html>
- [14] Gundlach J H and Merkowitz S M 2000 *Phys. Rev. Lett.* **85** 2869–72
- [15] Quinn T J, Speake C C, Richman S J, Davis R S and Picard A 2001 *Phys. Rev. Lett.* **87** 111101
- [16] Schwarz J P, Robertson D S, Niebauer T M and Faller J E 1998 *Science* **282** 2230–4
- [17] Tino G M 2003 *2001: a Relativistic Spacetime Odyssey* ed I Ciufolini *et al* (Singapore: World Scientific)
- [18] Young B, Kasevich M and Chu S 1997 *Atom Interferometry* ed P R Berman (New York: Academic) p 363
- [19] A laser cooling overview can be found in the Nobel lectures of Chu S 1998 *Rev. Mod. Phys.* **70** 685 Cohen-Tannoudji C N 1998 *Rev. Mod. Phys.* **70** 707 Phillips W D 1998 *Rev. Mod. Phys.* **70** 721
- [20] Bordé Ch J 2002 *Metrologia* **39** 435–63
- [21] Peters A 1998 *Dissertation* Department of Physics, Stanford University Peters A, Chung K Y and Chu S 2001 *Metrologia* **38** 25–61
- [22] Such a gradiometer has already detected the acceleration caused by nearby SMs: McGuiirk J M, Foster G T, Fixler J B, Snadden M J and Kasevich M A 2002 *Phys. Rev. A* **65** 033608
- [23] Petelski T, Fattori M, Lamporesi G, Stuhler J and Tino G M 2003 *Eur. Phys. J. D* **22** 279–83
- [24] Santarelli G, Clairon A, Lea S N and Tino G M 1994 *Opt. Commun.* **104** 339–44
- [25] Gibble K and Chu S 1993 *Phys. Rev. Lett.* **70** 1771–4 and references therein
- [26] Treutlein P, Chung K Y and Chu S 2001 *Phys. Rev. A* **63** 051401
- [27] Faller J E 2001 private communication
- [28] Santarelli G, Laurent Ph, Lemonde P, Clairon A, Mann A G, Chang S, Luiten A N and Salomon C 1999 *Phys. Rev. Lett.* **82** 4619–22